PCCP

Accepted Manuscript

This is an *Accepted Manuscript*, which has been through the Royal Society of Chemistry peer review process and has been accepted for publication.

Accepted Manuscripts are published online shortly after acceptance, before technical editing, formatting and proof reading. Using this free service, authors can make their results available to the community, in citable form, before we publish the edited article. We will replace this *Accepted Manuscript* with the edited and formatted *Advance Article* as soon as it is available.

You can find more information about *Accepted Manuscripts* in the **Information for Authors**.

Please note that technical editing may introduce minor changes to the text and/or graphics, which may alter content. The journal's standard **Terms & Conditions** and the **Ethical guidelines** still apply. In no event shall the Royal Society of Chemistry be held responsible for any errors or omissions in this *Accepted Manuscript* or any consequences arising from the use of any information it contains.

Journal Name

ARTICLE

Reducing optical losses in organic solar cells using microlens arrays: theoretical-experimental investigation of microlens dimensions

Yuqing Chen,[a,*] Moneim Elshobaki,[b,c,*] Ryan Gebhardt,[b,d,*] Stephen Bergeson,[e] Max Noack,[a] Joong-Mok Park,[d] Andrew C. Hillier,[f] Kai-Ming Ho,[d,e] Rana Biswas[d,e] and Sumit Chaudhary[a,b]

The performance of organic photovoltaic devices is improving steadily and efficiencies have now exceeded 10%. However, incident solar spectrum still largely remains poorly absorbed. To reduce optical losses, we employed a microlens array (MLA) layer on the side of the glass substrate facing the incident light; this approach does not interfere with the processing of the active-layer. We observed up to 10% enhancement in the short circuit current of poly({4,8-bis[(2-ethylhexyl)oxy]benzo[1,2-b:4,5-b′]dithiophene-2,6-diyl}{3-fluoro-2-[(2-ethylhexyl)carbonyl] thieno[3,4-b]thiophenediyl}):(6,6)-phenyl C71-butyric acid methyl ester (PTB7:PC$_{71}$BM) OPV cells. Theoretically and experimentally investigating several MLA dimensions, we found that photocurrent increases with the ratio of height to pitch size of MLA. Simulations reveal the enhancement mechanisms: MLA focuses light, and also increases the light path within the active-layer by diffraction. Photocurrent enhancements increase for a polymer system with thinner active-layers, as demonstrated in poly[N-9′-heptadecanyl-2,7-carbazole-alt-5,5-(4′,7′-di-2-thienyl-2′,1′,3′-benzothiadiazole)] (PCDTBT):PC$_{71}$BM OPVs with 17% improvement in short circuit current.

Introduction

Solar-electric conversion using organic semiconductors has been a very active research area within the photovoltaic community. Organic photovoltaics (OPVs) have the advantages of flexibility, light weight, and potentially low cost roll-to-roll production.[1] In the last decade, power conversion efficiency (PCE) of OPVs has increased from 2% to 11%.[2, 3] The rapid improvement of PCE has primarily been due to the following aspects: (1) new materials, especially small band-gap donor polymers with appropriate energy level offsets to the fullerene acceptors,[4-6] (2) improved anodic and cathodic buffer layers,[7-9] and (3) the optimization of the bulk-heterojunction morphology using approaches such as annealing and additives.[10-14] Although the OPV efficiencies have improved steadily, they still are lower than those of contemporary thin-film inorganic solar cells. The efficiency losses in OPV cells include thermalization, exciton recombination, energy losses required for exciton dissociation, charge-carrier recombination, and optical losses. Among them, optical losses have been estimated to be nearly 40% of total losses.[15] This is primarily because the thicknesses of OPV active-layers, as optimized for efficient charge transport, are only 100-200 nm or less. Therefore,

methodologies to improve light absorption are necessary for further advancement of OPV technology.

In addition to tailoring the band-gap of materials to absorb more solar spectrum, several device architectural approaches have been explored to improve light absorption in OPVs. These include utilizing textured substrates[16-18], substrates with wrinkles and deep folds[19], metal nanoparticles in or adjacent to the active-layers[20, 21] and patterning the active-layers[22]. However, these approaches bring along several challenges and bottlenecks. In the textured substrate approach of Nalwa et al.,[16] texture dimensions need to be tailored, or rather discovered by trial-and-error for conformal coating of active-layers. Low-aspect ratio structures lead to over-filling of trenches and increased charge-carrier recombination, and high-aspect ratio structures lead to catastrophic shunts between the electrodes. Additionally, for contemporary polymer systems, which typically have thinner active-layers, achieving conformal coatings will be more challenging. Overall, conformally patterned cells may have good theoretical performance for optimum optical designs,[18] but realizing conformal coatings by solution-processing is non-trivial and an open problem. The microprism approach,[17] and the one of utilizing substrates with wrinkles and deep folds[19] suffer from similar issues. In the latter, it is also challenging to have a quantitative and precise

control on the dimensions of self-assembled wrinkles and folds. Incorporating metal nanoparticles in or adjacent to the active-layer can also improve light absorption by surface plasmon polarization assisted field enhancement, and lateral propagation of light in the plasmonic mode.[20, 21, 23-25] However, metal nanoparticles are centers for exciton quenching and charge-carrier recombination. In summary, all of the above approaches are intrusive to the active-layer, and optical enhancement often comes at a cost of disrupting the charge dynamics.

An alternative non-intrusive approach is employing microlens array (MLA) on the side of the transparent substrate opposite to the active-layer, such that light traverses the MLA and transparent substrate before entering the active-layer. Being on the other side, MLAs do not affect the fabrication or morphology of the active-layer. The MLA approach has been successfully used in organic light-emitting diodes to enhance light extraction[26-29]. More recently, MLA approach was also demonstrated to be useful for OPVs. Myers *et al.* utilized hemispherical microlenses with 100μm diameter;[30] this led to refraction of light towards the active-layer and reduced surface reflection. Since the light was no longer traveling perpendicular to the substrate, the overall path length inside the active layer was increased and thus the absorption increased. In our previous publication,[31] we showed that MLA with smaller features sizes can be more promising because besides reduced surface reflection and refraction, they can also benefit from diffraction. In that report, we only investigated 2μm diameter microlenses, but by smaller feature sizes we more generally mean feature sizes in or near the regime of optical wavelengths. Feature sizes (diameters) smaller than 2μm have not been explored; neither has been the effect of changing the height of microlenses. That is the focus of this report, in which we show that both the pitch and height of microlens structures critically affect the device performance. We couple experimental investigations with theoretical predictions, for two contemporary polymer systems (PTB7 and PCDTBT). Simulations also elucidate the mechanisms behind enhancement in light-absorption.

Methods

Microlens array fabrication

Periodic MLA with square lattice symmetry, having a structure similar to a closely packed egg tray, was fabricated by soft lithography imprinting on polyurethane (Summer Optical Lens Bond Type J-91) from a polydimethylsiloxane (PDMS) mold. Polyurethane was then cured under UV light for 3 hours, forming a solid MLA pattern after peeling off the PDMS mold. The polyurethane has negligible absorption for wavelengths greater than 300 nm. In addition, the operating temperature range of -50 to 110°C is suitable for photovoltaic applications. MLAs with different pitches were fabricated from PDMS molds of different pitches. The PDMS molds with varying pitches and the desired inverse relief patterns were obtained from holographic interference lithography of photoresist. Further details about fabrication of MLA pattern and PDMS molds are described elsewhere.[32, 33] The fabricated MLA with different pitch sizes can be seen in Fig. 1.
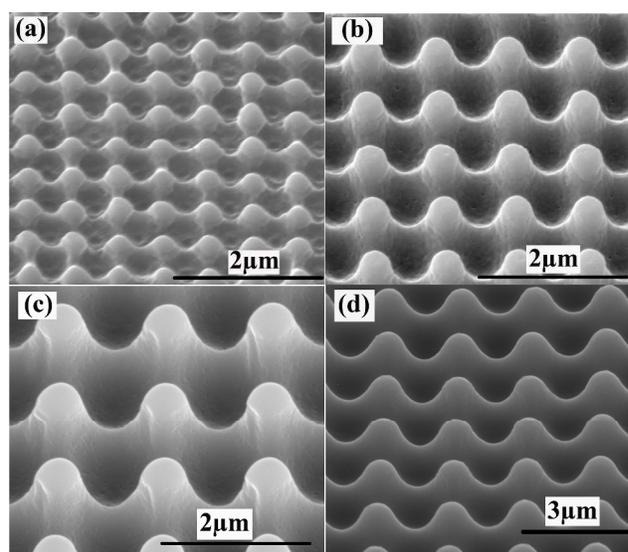
Fig. 1 SEM images of MLAs with pitch sizes (a) 0.6μm, (b) 1μm, (c) 1.5μm, and (d) 2μm.

Device fabrication

PTB7 (1-Material) and PC$_{71}$BM (1-Material) with a weight ratio 1:1.5 were dissolved in 1,2-dichlorobenzene:1,8-diiodoctane (97%:3% by volume) with 25 mg/ml total concentration, and stirred at 800 rpm on a hot plate at a temperature of 60 °C for around 20 hours. Indium Tin Oxide (ITO) coated glasses (Delta Technologies) with and without MLA pattern were pre-cleaned by sonicating in 2-propanol/acetone and then de-ionized water for 10 min each. The substrates were then dried with nitrogen and exposed to air plasma for 1 minute. Poly (3, 4-ethylenedioxythiophene):poly (styrenesulfonate) (PEDOT:PSS) was spin-coated on ITO substrates at 4000 rpm for 60 s, followed by annealing on a hot plate at 120 °C for 10 min. The substrates were then transferred inside a nitrogen-filled glovebox. The previously prepared active-layer solution was filtered through a 0.2 μm filter, dropped on the PEDOT:PSS coated ITO, and spin-coated at 1000 rpm for 60 s. After spin-coating, the devices were covered with separate petri dishes for two hours. This length of time was long enough to dry the active-layers. To finish the device fabrication, 20 nm calcium and 100 nm aluminium were thermally evaporated on the active-layer at a pressure of around 10^{-6} mbar. The preparation of substrates for PCDTBT based devices was done similar to that of PTB7. PCDTBT of molecular weight 50 kDa was purchased from 1-Material. M$_O$X (99.99%) and LiF (99.98%) were purchased from Sigma Aldrich. For the PCDTBT:PC$_{71}$BM system, 10 nm of MoO$_X$ anodic buffer layer was thermally evaporated on ITO under a vacuum of about 10^{-6} mbar at the rate of 0.5 Å/sec. Solution of PCDTBT and PC$_{71}$BM (1:3.5, w/w), with a concentration of 7 mg/mL in 1,2-dichlorobenzene, was continuously stirred on a hot plate at 90 °C and 650 rpm for 8 hours. The temperature of the solution was then reduced to 60 °C at the same stirring speed. After that, the active-layer was deposited on the top of the MoO$_X$ anodic layer at 2000 rpm for 45 seconds. The films were then dried under petri dishes for 20 min, and then

annealed for 15 min on a hot plate at 70 ^{o}C. Finally, LiF (2 nm) and Al (100 nm) were thermally evaporated on the active-layer at the rates of 0.5 and 8 Å/sec, respectively. PTB7 and PCDTBT based device architectures without and with MLA are depicted in Fig. 2.
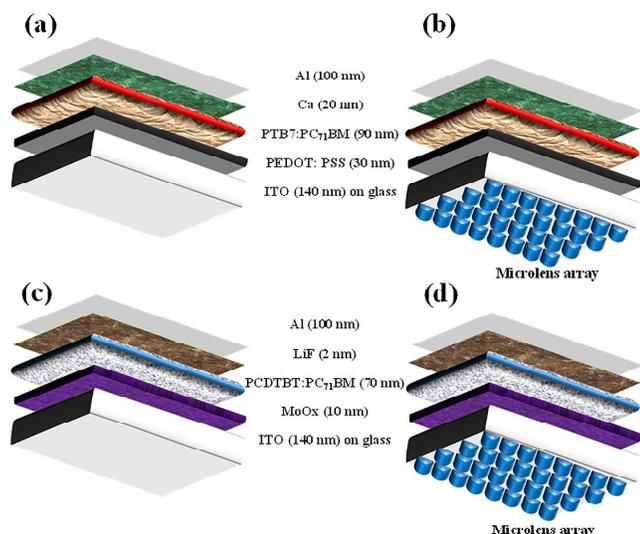
Fig. 2 Schematic diagrams of different devices: (a) PTB7 reference device, (b) PTB7 MLA device, (c) PCDTBT reference device, (d) PCDTBT MLA device.

Experimental Characterization

For global transmission measurements, 0% and 100% were first calibrated for the integrating sphere. ITO coated glass substrates with and without MLA were placed in front of the opening of integrated sphere with ITO layer facing the opening. Then global transmission spectra were recorded from the optical fiber coupled spectrometer (Ocean Optics). For current density-voltage characterization, ELH Quartzline halogen lamp provided 1 sun illumination after being calibrated with a reference crystalline Si solar cell coupled with a KG-5 filter. All the samples were measured under the same light intensity. In order to measure external quantum efficiency (EQE), a 100 W halogen bulb (OSRAM Bellaphot) was used as a light source with a single grating monochromator (Horiba Jobin Yvon Srl). An optical chopper (Thor Labs) coupled with a lock-in amplifier (Standford Research Systems) was employed to reduce system noise. The EQE spectra were calculated after comparing the sample signal to the crystalline Si reference signal. Light angle dependent current density was measured using a customized setup in the lab. 1 sun illumination was obtained using a light source (LS150 Abet technology) and calibrated with a reference crystalline Si solar cell. A rotating sample stage was used to change the incident angles from 0 to 80 degrees, and short-circuit current was measured using Keithley 2400 sourcemeter.

Simulations

We used the rigorous scattering matrix (SM) method[34, 35] where Maxwell's equations are solved in Fourier space, i.e. in a basis of plane waves for both polarizations. We divided the OPV devices into slices in the *z*-direction, wherein the dielectric function depends periodically on *x* and *y* in each slice i.e. the in-plane coordinates *r=(x,y)*. The dielectric function ε has Fourier components ε(**G**) given by

$$\varepsilon(\boldsymbol{r}) = \sum_G \varepsilon(\boldsymbol{G}) \exp(i\boldsymbol{G}.\boldsymbol{r}) \qquad (1)$$

where **G** are reciprocal lattice vectors. The electric **E** and magnetic (**H**) fields are also expanded in Fourier components of strength **e** and **h,** which are functions of **G** and z.

$$\boldsymbol{E}(\boldsymbol{r}) = \sum_G \boldsymbol{e}(\boldsymbol{G}, z) \exp(-i(\boldsymbol{k}+\boldsymbol{G}).\boldsymbol{r}) \qquad (2)$$

$$\boldsymbol{H}(\boldsymbol{r}) = \sum_G \boldsymbol{h}(\boldsymbol{G}, z) \exp(-i(\boldsymbol{k}+\boldsymbol{G}).\boldsymbol{r}) \qquad (3)$$

where k is a Bloch vector. We solve an eigenvalue equation for the transverse x and y components of the fields **e**, **h** in each layer[34]. We obtain the SM for each layer by solving the Maxwell's equations with the boundary conditions, that the parallel components of the fields **e**, and **h** are continuous at each interface. The SM of each layer was combined by a standard convolution procedure[34] to obtain the SM of the entire structure, which relates the incoming (incident) fields to the outgoing (reflected and transmitted) fields. The SM yields the total reflectance R (including diffraction), transmittance T (~0) and absorbance A (= 1 − R − T) at each wavelength. This SM technique has advantages over real-space methods in being able to simulate fully 3-dimensional geometries, without added memory requirements, since a real space grid is unnecessary. The SM method is fully parallelized with each frequency being sent to a different processor, and we have efficiently simulated[18,36] complex textured organic solar cells with this method. The results are well converged for N_G=270-300 plane waves (G vectors) for each polarization of the field, leading to a scattering matrix size of order 540-600 ($2N_G$). Our simulations utilize experimental values for the wavelength dependent dielectric functions for the materials including measurements for PCDTBT[37] and PTB7[38], and standard tabulated values for other materials[39].
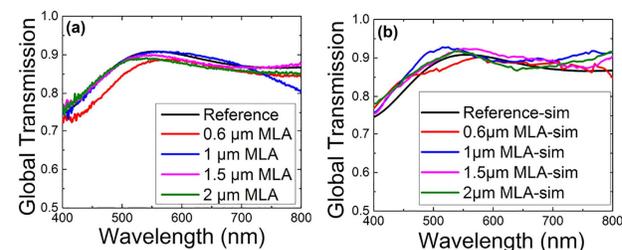
Fig. 3 (a) Experimental and (b) simulated global transmission spectra of substrates without MLA (Reference) and with MLA (0.6 µm, 1 µm, 1.5 µm and 2 µm pitches).

Results and Discussion

MLAs with four pitch sizes (0.6 µm, 1 µm, 1.5 µm, and 2 µm) were fabricated and evaluated. In order to compare the optical properties of the substrates with and without MLA, the global transmission spectra of these substrates (structure: MLA/glass/ITO) were measured as well as simulated; they are plotted in Fig. 3. As the experimental plots in Fig. 3(a) show, all substrates have similar spectra; only the 0.6 µm MLA substrate showed slightly lower transmission between 400 nm and 550 nm wavelengths. This lower transmission is due to stronger scattering of light passing through the 0.6 µm pitch microlenses. We visually observed that part of the scattered light escaped out through the side of the substrates before entering the integrating sphere. The 1 micron case also differs from simulation, showing a decrease at longer wavelengths. This could be due to a similar issue of light scattering at high angles and escaping the integrating sphere aperture. The global transmission of all of the MLAs were comparable. The calculated spectra from simulation support this conclusion. The calculated spectra in Fig. 3(b) are very similar to the experimental data. All substrates have similar global transmission spectra including 0.6 µm MLA substrate, since calculations include the scattered light that escaped in the experiment. The positions of maxima are near 530 nm from multiple interference effects, depending on ITO thickness (Fig. S1 in ESI†). Even though all these substrates had similar global transmission spectra, they exhibited very different diffraction patterns. These patterns are shown in the photographs of Fig. 4. To obtain these images, devices were illuminated with a white light beam normal to the substrates, through a hole at the bottom. A sheet of white paper was placed next to the devices to project the diffraction patterns. No diffraction pattern was observed for the reference device. The MLA substrates, however, being two-dimensional diffraction gratings, showed rainbow like diffraction patterns. According to the grating equation $dsin\theta_m = m\lambda$, diffraction order m is directly proportional to grating period d. Thus, larger period (pitch) leads to additional diffraction modes. On the other hand, diffraction angle θ_m is inversely proportional to the pitch. Thus, larger pitch leads to decreased spacing between different diffraction orders. Both, additional modes and decreased angles for larger pitches are evident in the photographs of Fig. 4.
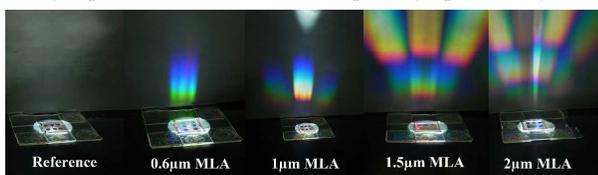
Fig. 4 Photographs of light diffraction patterns through reference and MLA devices.

Fig. 5 (a) *JV* curves, and (b) EQE spectra of PTB7 reference and MLA devices (p = 0.6 µm, h = 250 nm; p = 1 µm, h = 350 nm; p = 1.5 µm, h = 900 nm; p = 2 µm, h = 1000 nm).

To characterize the effect of MLAs on the performance of OPVs, PTB7:PC$_{71}$BM devices were fabricated on the reference substrate (no MLA) and substrates with MLA of different pitch sizes. Current versus voltage measurements were performed under illumination; the results are plotted in Fig. 5(a). Open circuit voltages of MLA devices were similar to the reference. However, short circuit current densities (J_{sc}) of all MLA devices were notably higher than the reference. As tabulated in table 1, J_{sc} and PCE of the reference were 16.1 mA/cm^2 and 7.73%, respectively, among the highest in literature for PTB7 based devices. Variation of the enhancement is shown in boxplots in Fig S2. Among the MLA devices, devices with 1 µm pitch MLA showed the highest J_{sc} and PCE, 18 mA/cm^2
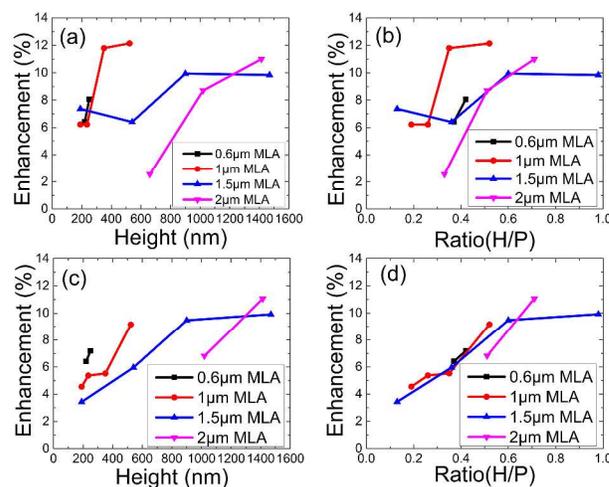
Fig. 6 Enhancement of J_{sc} of PTB7:PC$_{71}$BM devices for MLA of different pitch sizes as a function of height and height-pitch ratio of MLA: (a, b) experimental results; (c, d) simulation results.

Table 1 J_{sc} and PCE of PTB7:PC$_{71}$BM OPV devices for MLAs of different pitch sizes.

Parameters	Reference	0.6 µm (H=250nm)	1 µm (H=350nm)	1.5 µm (H=900nm)	2 µm (H=1000nm)
J_{sc} (mA/cm^2)	16.10	17.39	18.00	17.70	17.50
J_{sc} enhancement (%)		8.01	11.80	9.94	8.70
PCE (%)	7.73	8.14	8.55	8.25	8.25
PCE enhancement (%)		5.30	10.60	6.73	6.73

and 8.55%, respectively. J_{sc} and PCE increased going from 0.6 μm pitch MLA to 1 μm pitch MLA, and then slightly decreased for 1.5 μm and 2 μm pitch MLA. The values of heights of all MLAs are also listed in table 1. EQE spectra of the reference and MLA devices are plotted in Fig. 5(b). As can be seen, MLA devices exhibit broadband enhancement across the range of wavelengths absorbed by the PTB7:PC$_{71}$BM system, especially in the 400 - 500 nm and 600 - 800 nm wavelength regions.

In addition to the pitch sizes, heights of microlenses also affected the OPV device performance (Fig. 6). To investigate the effect of heights, two to four height values were evaluated experimentally for each pitch. Optical simulations for these dimensions were also performed on corresponding device structures. Different heights for each pitch were realized by intuitive variation of photoresist spin-coating parameters during MLA fabrication; all the heights for a given pitch were such that the height/pitch ratio (h/p ratio) was ≤ 1. Fig. 6 shows the combined (experimental and simulated) J_{sc} enhancement data for different pitches and heights; enhancement versus height to pitch ratio (h/p ratio) are also plotted. As can be seen, for a given pitch, mostly enhancement increased as the height of MLAs increased.

First, we discuss the experimental results of height variations (Fig. 6(a), (b)). For the 0.6 μm pitch MLA device, J_{sc} enhancement was 6-8% around h/p ratio of 0.4. For the 1 μm pitch MLA device, there was a significant jump in enhancement from 6% to 12% when the h/p ratio increased from 0.2 to 0.4, following which the enhancement began to saturate. The enhancement values increased less sharply with height in the 1.5 μm pitch MLA device; enhancement was ~7% for smaller h/p ratios (0.2 - 0.4), and ~10% for higher h/p ratios (0.6 − 1). In the devices with the largest MLA pitch of 2 μm, the enhancement increased rapidly with increasing h/p ratio, similar to the 1 μm pitch MLA devices. Around the h/p ratio of 0.3, the enhancement was 2.5%, while it increased to 9% at the ratio of 0.5, and to the highest value of 11% at the ratio of 0.7.
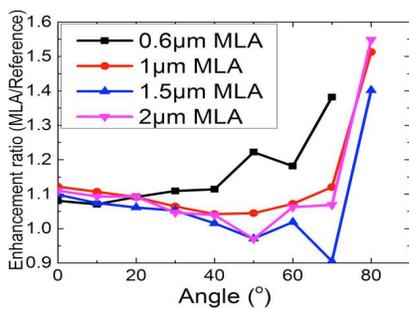
Fig. 7 The J_{sc} enhancement ratio of MLA devices to reference vs. incident light angle.

Simulations agree with the experiments on a general trend that for a given MLA pitch, enhancement increases as height increases (Fig. 6 (c), (d)). On the absolute enhancement values, there are some differences between experiments and simulations, which can be due to differences in the MLA structure employed in simulations and the one actually realized

by fabrication. Fabricated structures have some unintentional imperfections and local irregularities, examples of which are some depressions in the valleys, as can be seen in SEM images (Fig. 1). Nevertheless, simulations agree with measurements on the central trend that enhancement increases with increasing h/p ratio. Simulations also reveal an interesting feature relevant for
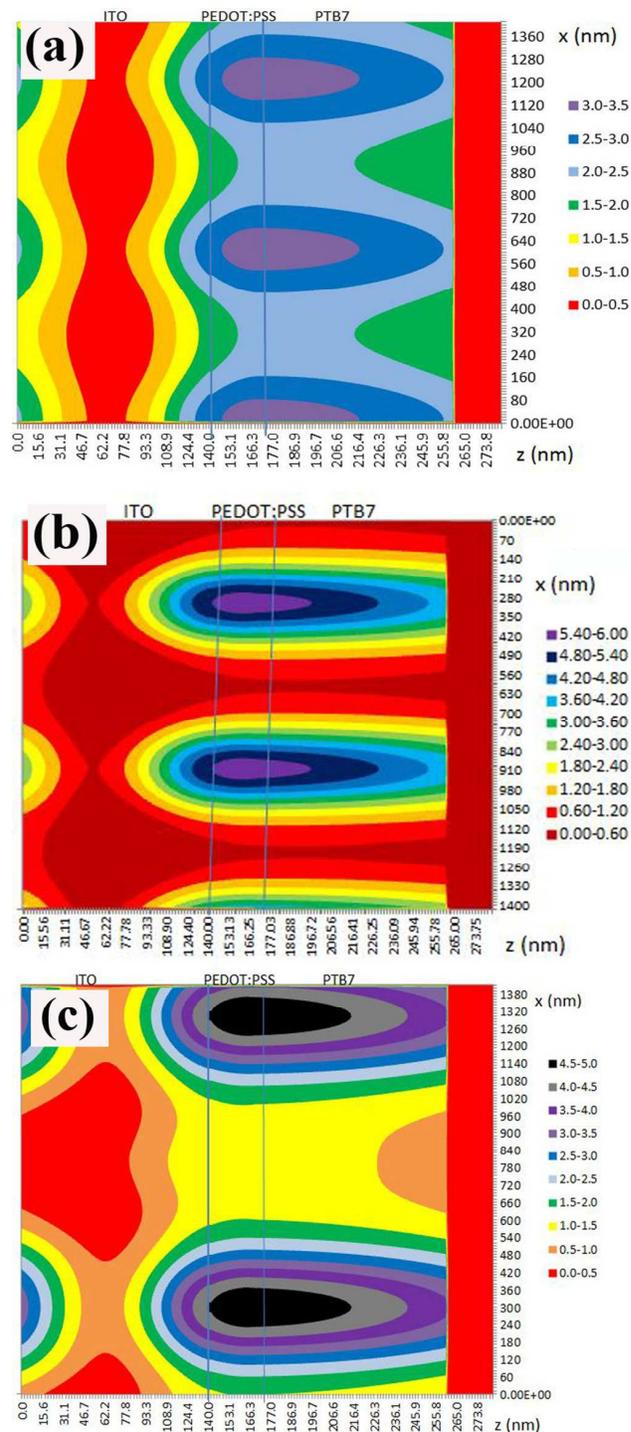
Fig. 8 Simulated electrical field distribution (for wavelength 610 nm) inside the MLA devices with (a) p = 0.6 μm, h = 600 nm, (b) p = 0.6 μm, h = 1000 nm, (c) p = 1 μm, h = 1000 nm.

MLA architecture design: that across different MLA pitches, enhancement values are similar or close for a given h/p ratio. The h/p ratio around 0.4 is a pronounced example of this.

The current-voltage measurements under illumination are typically done with incident light normal to the substrates. However, for non-tracking PV systems, incident angle of sunlight changes throughout the day. In order to probe the angle dependence, we carried out current-voltage measurements with different incident light angles. Devices were rotated from the normal angle (0°) to almost parallel to the light source beam (80°), and J_{sc} was measured at 10° intervals. Angle dependent enhancement ratios were obtained by dividing J_{sc} of MLA devices by that of the reference device (Fig. 7). For the MLA devices with 1 μm, 1.5 μm and 2 μm pitch, enhancement slightly decreases with increasing angle up to 50°. This is because with increasing angle, light path in the reference device increases as the reflectance (Rp) of p-polarized light decreases, vanishing at the well-known Brewster angle of 50° for glass. At higher angles above the Brewster angle the reflectance (Rp) increases again for the reference and increasingly less light is absorbed in the active-layer. In contrast, MLA reduces the reflection and enhancement ratios in MLA devices rapidly rise to 1.4 - 1.5 at 80°. The enhancement ratio for 0.6 μm pitch MLA device showed a consistently increasing trend as incident light angle increased, different from devices of other pitch sizes. This might be due to diffraction effects being strongest in the 0.6 μm device. The angle dependence trends had no evident correlation with heights as the h/p ratios of MLA devices were 0.4, 0.5, 1 and 0.7 (for 0.6, 1, 1.5 and 2 μm pitch MLAs, respectively).
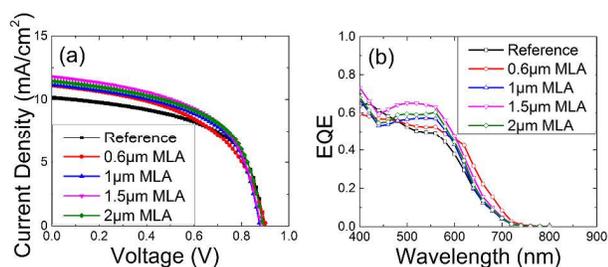
Fig. 9 (a) *JV* curves and (b) EQE spectra of PCDTBT based reference and MLA devices.

To better understand the enhancement mechanisms in MLA devices, electrical field distributions in MLA devices were simulated for different MLA dimensions. Fig. 8 shows the electrical field distribution for 610 nm wavelength in the 0.6 μm and 1 μm pitch MLA devices. To probe the height

dependence, two heights were simulated for the 0.6 μm pitch MLA device. One can see that field intensities in the PTB7:PC$_{71}$BM active layers exhibit a periodic distribution of high intensity focused regions. The incident electrical field intensity was 1. In the 0.6 μm pitch MLA devices (Fig. 8(a), (b)), as the MLA height increases from 600 nm to 1000 nm, the light focusing increases, which contributes to higher electrical field intensity in the higher height device. However, as the field intensities at the periodic focused spots gets higher, the field intensities in the intermediate regions decrease, even below 1 in some regions. However, overall there is a gain. Comparing Fig. 8(b) and Fig. 8(c), the MLA height in these two devices is the same at 1000 nm, but (b) has a smaller pitch of 0.6 μm than (c) of 1μm. The maximum field intensity of (b) is slightly larger than that of (c), which agrees with the observed phenomena. Although the focusing regions are closer for the 0.6 μm pitch, portions of the enhanced $|E|^2$ lie in the PEDOT:PSS layer. Thus, there is a trade-off between the spatial separation of the focusing spots dictated by the pitch and the location of the focus spots within the active layer. The balance of this trade-off determines the optimal MLA configuration.

In OPVs based on several contemporary polymers, optimal thicknesses of active-layer are smaller as optimized for charge transport; for example, 60~70 nm thickness in devices based on PCDTBT. We also fabricated MLA and reference devices with PCDTBT polymer. Current-voltage and EQE curves of these devices are plotted in Fig. 9 and performance parameters are listed in table 2. MLA devices showed very similar open circuit voltage to the reference. However, the J_{sc} of all MLA devices was higher than the reference. As shown in table 2, the reference has J_{sc} of 10.03 mA/cm^2, and PCE of 5.19%. MLA devices showed improvement in J_{sc} by between 10.47% for 0.6 μm MLA to 10.67% for 1 μm pitch MLA. As MLA pitch increased to 1.5 μm, the enhancement increased to 16.95% and then dropped to 13.86% for 2 μm pitch MLA. The enhancement of PCE in MLA devices also increased from 5.59% for 0.6 μm pitch to 7.71% for 1 μm pitch, and then peaks to 13.10% for 1.5 μm and drops to 11.56% for 2 μm MLA. EQE data shows that the MLAs (1μm, 1.5 μm and 2μm) mainly have enhancement in wavelength region of 480 nm – 800 nm. However, there is a drop for wavelengths between 400 nm and 460 nm. The enhancement from the 0.6 μm MLA is higher in the longer wavelength region of 600 nm – 800 nm than the other MLAs. These results, together with the PTB7 results discussed previously, show that OPV systems with very thin active layers suffer from poor absorption efficiency and can greatly benefit from optical enhancement schemes.

Table 2 J_{sc} and PCE of PCDTBT:PC$_{71}$BM OPV devices for MLAs of different pitch sizes.

Parameters	Reference	0.6 μm (H=250nm)	1 μm (H=350nm)	1.5 μm (H=900nm)	2 μm (H=1000nm)
J_{sc} (mA/cm^2)	10.03	11.08	11.10	11.73	11.42
J_{sc} enhancement (%)		10.47	10.67	16.95	13.86
PCE (%)	5.19	5.48	5.59	5.87	5.79
PCE enhancement (%)		5.59	7.71	13.10	11.56

Conclusions

We demonstrate that by adding a MLA layer on the light-facing side of the transparent substrate in OPV devices, optical absorption in the active-layers improve due to reduced reflection, and increased light path achieved by light focusing and diffraction. Optical field intensity increases at periodical spots inside the active layer. All of these effects combine to enhance short-circuit currents and power conversion efficiencies. We get around 10% enhancements in PTB7:PC_{71}BM devices with MLA pitch size of 0.6 µm, 1 µm, 1.5 µm and 2 µm, even when the reference devices were high efficiency devices with optimized processing conditions. The enhancement generally increases with increasing height of microlenses. When the angle of light incidence changes away from the normal, the enhancements for 1 µm, 1.5 µm or 2 µm pitch MLAs drop slightly, and then increase significantly at large angles. For 0.6 µm pitch MLA, enhancement increases at all non-normal angles. Simulations using the scattering matrix approach support the central experimental observations and provide insights into the enhancement mechanisms. The enhancement was as high as 17% in PCDTBT based MLA devices. The simple stamping technique to fabricate the MLAs can be scaled readily to larger areas. Moreover, the MLA is on the substrate side opposite to the active layer and does not hinder the cell fabrication or electrical characteristics. It is also generally applicable to all types of solar cells due to its non-intrusive and external nature.

Acknowledgements

Notes and references

* These authors contributed equally to this work

a Department of Electrical and Computer Engineering, Iowa State University, Ames, Iowa 50011, USA. Email: sumitc@iastate.edu; Tel: +1-515-294-0606; Fax: +1-515-292-8432

b Department of Materials Science and Engineering, Iowa State University, Ames, Iowa 50011, USA

c Physics Department, Faculty of Science, Mansoura University, Mansoura 35516, Egypt

d Ames Laboratory - USDOE, Ames, Iowa 50011, USA

e Department of Physics and Astronomy, Iowa State University, Ames, Iowa 50011, USA

f Department of Chemical and Biological Engineering, Iowa State University, Ames, Iowa 50011, USA

References

1. R. Gaudiana and C. Brabec, *Nat Photonics*, 2008, **2**, 287.
2. Z. He, C. Zhong, S. Su, M. Xu, H. Wu and Y. Cao, *Nat Photonics*, 2012, **6**, 593.
3. NREL, Best Research Cell Efficiency Records, http://www.nrel.gov/ncpv/images/efficiency_chart.jpg.
4. D. Gendron and M. Leclerc, *Energ Environ Sci*, 2011, **4**, 1225.
5. S. Günes, H. Neugebauer and N. S. Sariciftci, *Chem Rev*, 2007, **107**, 1324.
6. R. Kroon, M. Lenes, J. C. Hummelen, P. W. M. Blom and B. de Boer, *Polym Rev*, 2008, **48**, 531.
7. H.-L. Yip and A. K. Y. Jen, *Energ Environ Sci*, 2012, **5**, 5994.
8. E. L. Ratcliff, B. Zacher and N. R. Armstrong, *J Phys Chem Lett*, 2011, **2**, 1337.
9. R. Po, C. Carbonera, A. Bernardi and N. Camaioni, *Energ Environ Sci*, 2011, **4**, 285.
10. J. A. Carr, Y. Chen, M. Elshobaki, R. C. Mahadevapuram and S. Chaudhary, *Nanomaterials and Energy*, 2011, **1**, 18.
11. J. Jo, S.-S. Kim, S.-I. Na, B.-K. Yu and D.-Y. Kim, *Adv Funct Mater*, 2009, **19**, 866.
12. M. Campoy-Quiles, T. Ferenczi, T. Agostinelli, P. G. Etchegoin, Y. Kim, T. D. Anthopoulos, P. N. Stavrinou, D. D. C. Bradley and J. Nelson, *Nat Mater*, 2008, **7**, 158.
13. G. Li, V. Shrotriya, Y. Yao, J. Huang and Y. Yang, *J Mater Chem*, 2007, **17**, 3126.
14. H. Hoppe and N. S. Sariciftci, *J Mater Chem*, 2006, **16**, 45.
15. T. Kirchartz, K. Taretto and U. Rau, *J Phys Chem C*, 2009, **113**, 17958.
16. K. S. Nalwa, J.-M. Park, K.-M. Ho and S. Chaudhary, *Adv Mater*, 2011, **23**, 112.
17. M. Niggemann, M. Glatthaar, P. Lewer, C. Muller, J. Wagner and A. Gombert, *Thin Solid Films*, 2006, **511**, 628.
18. R. Biswas and E. Timmons, *Opt Express*, 2013, **21**, A841.
19. J. B. Kim, P. Kim, N. C. Pegard, S. J. Oh, C. R. Kagan, J. W. Fleischer, H. A. Stone and Y.-L. Loo, *Nat Photonics*, 2012, **6**, 327.
20. D. Duche, P. Torchio, L. Escoubas, F. Monestier, J.-J. Simon, F. Flory and G. Mathian, *Sol Energy Mater Sol Cells*, 2009, **93**, 1377.
21. H. Shen, P. Bienstman and B. Maes, *J Appl Phys*, 2009, **106**, 073109.
22. J. You, X. Li, F.-x. Xie, W. E. I. Sha, J. H. W. Kwong, G. Li, W. C. H. Choy and Y. Yang, *Adv Energy Mater*, 2012, **2**, 1203.
23. S. Vedraine, P. Torchio, D. Duché, F. Flory, J.-J. Simon, J. Le Rouzo and L. Escoubas, *Sol Energy Mater Sol Cells*, 2011, **95, Supplement 1**, S57.
24. A. J. Morfa, K. L. Rowlen, T. H. Reilly, M. J. Romero and J. van de Lagemaat, *Appl Phys Lett*, 2008, **92**, 013504.
25. S.-S. Kim, S.-I. Na, J. Jo, D.-Y. Kim and Y.-C. Nah, *Appl Phys Lett*, 2008, **93**, 073307.
26. F. Galeotti, W. Mróz, G. Scavia and C. Botta, *Org Electron*, 2013, **14**, 212.
27. J. B. Kim, J. H. Lee, C. K. Moon, S. Y. Kim and J. J. Kim, *Adv Mater*, 2013, **25**, 3571.
28. Y. Sun and S. R. Forrest, *J Appl Phys*, 2006, **100**, 073106.
29. E. Wrzesniewski, S.-H. Eom, W. Cao, W. T. Hammond, S. Lee, E. P. Douglas and J. Xue, *Small*, 2012, **8**, 2647.
30. J. D. Myers, W. Cao, V. Cassidy, S.-H. Eom, R. Zhou, L. Yang, W. You and J. Xue, *Energ Environ Sci*, 2012, **5**, 6900.
31. Y. Chen, M. Elshobaki, Z. Ye, J.-M. Park, M. A. Noack, K.-M. Ho and S. Chaudhary, *Phys Chem Chem Phys*, 2013, **15**, 4297.
32. J.-M. Park, Z. Gan, W. Y. Leung, R. Liu, Z. Ye, K. Constant, J. Shinar, R. Shinar and K.-M. Ho, *Opt Express*, 2011, **19**, A786.
33. X.-C. Yuan, W. X. Yu, M. He, J. Bu, W. C. Cheong, H. B. Niu and X. Peng, *Appl Phys Lett*, 2005, **86**, 114102.
34. Z.-Y. Li and L.-L. Lin, *Physical Review E*, 2003, **67**, 046607.
35. R. Biswas and C. Xu, *Opt Express*, 2011, **19**, A664.